Analysis of Nonlinear Behavior of Power HBTs

Woonyun Kim, *Member, IEEE*, Sanghoon Kang, Kyungho Lee, Minchul Chung, Jongchan Kang, and Bumman Kim, *Senior Member, IEEE*

***Abstract*—To accurately understand the linear characteristics of a heterojunction bipolar transistor (HBT), we developed an analytical nonlinear HBT model using Volterra-series analysis. The model considers four nonlinear components: r_π, $C_{\rm diff}$, $C_{\rm depl}$, and g_m. It shows that nonlinearities of r_π and $C_{\rm diff}$ are almost completely canceled by g_m nonlinearity at all frequencies. The residual g_m nonlinearity is highly degenerated by input circuit impedances. Therefore, r_π, $C_{\rm diff}$, $C_{\rm depl}$, and g_m nonlinearities generate less harmonics than C_{bc} nonlinearity. If C_{bc} is linearized, g_m is the main nonlinear source of HBT, and $C_{\rm depl}$ becomes very important at a high frequency. The degeneration resistor R_E is more effective than R_B for reducing g_m nonlinearity. This analysis also shows the dependency of the third-order intermodulation (IM3) on the terminations of the source second harmonic impedances. The IM3 of HBT is significantly reduced by setting the second harmonic impedances of $Z_{S,2\omega_2} = 0$ and $Z_{S,\omega_2-\omega_1} = 0$.**

***Index Terms*—Heterojunction bipolar transistors, intermodulation distortion, nonlinearity.**

I. Introduction

THE transmitters of the handsets of digital mobile communication systems require highly efficient linear power amplifiers [1]–[4]. Heterojunction bipolar transistors (HBTs) are widely used for the amplifiers and their nonlinear behavior has been extensively studied [4]–[12]. It is commonly known that C_{bc} is the dominant nonlinear source and should be linearized to reduce intermodulation distortions [7], [9]–[13]. C_{bc} is a depletion capacitance and is a rather moderate nonlinear component, which is surprising since HBT has highly nonlinear sources. The dependence of the HBTs base current i_B on base-to-emitter voltage v_{BE} is an exponential function, one of the strongest nonlinearities found in nature. The same is true of its collector current, i_C, which is basically similar to i_B. Furthermore, the junction capacitance, which is primarily a diffusion capacitance, is also strongly nonlinear. These exponential nonlinear behaviors are not seen in the nonlinear characteristics of HBT. Thus, the measured high linear characteristics of HBT have motivated many researchers to study the intermodulation (IM) mechanism of HBT. The good linearity of HBT was attributed to the partial cancellation between the IM currents generated from the exponential junction current and the junction capacitance [5], or the partial cancellation of IM currents from the total base-emitter current and the total base–collector current [8]. According to reference [10], it resulted from the almost complete cancellation between the output nonlinear currents generated by the emitter–base and base–collector current sources. It was also reported that the emitter and base resistances linearize HBT output [9]. Differing descriptions for the linear characteristics make it necessary for a more complete explanation. To more accurately gauge the characteristics of an HBT, an analytical nonlinear HBT model, using Volterra-series analysis, was developed [14], [15]. Based on the model, the fundamental nonlinear behavior of an HBT is simulated and its physical characteristics are clearly described.

Manuscript received February 28, 2001. This work was supported in part by the Agency for Defense Development and in part by the Ministry of Education under the Brain Korea 21 Project.

W. Kim was with the Pohang University of Science and Technology, Pohang 790-784, Korea. He is now with the RFIC Design Group, System LSI Business, Samsung Electronics Company Ltd., Giheung 449-711, Korea (e-mail: kwnkwn@samsung.co.kr).

S. Kang, K. Lee, M. Chung, and J. Kang are with the Department of Electronic and Electrical Engineering and Microwave Application Research Center, Pohang University of Science and Technology, Pohang 790-784, Korea.

B. Kim is with the Department of Electrical Engineering, California Institute of Technology, Pasadena, CA 91125 USA, on leave from the Department of Electronic and Electrical Engineering and Microwave Application Research Center, Pohang University of Science and Technology, Pohang 790-784, Korea (e-mail: bmkim@postech.ac,kr).

Publisher Item Identifier 10.1109/TMTT.2002.800396.

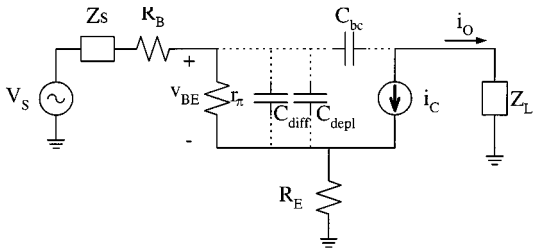

Fig. 1. HBT equivalent circuit with dotted capacitances for a high-frequency operation.

II. Basic Description of Bipolar Junction Transistor (BJT) Linear Characteristics

Fig. 1 shows the equivalent circuit of a BJT with base and emitter degeneration resistances R_B and R_E. At a low frequency, the capacitive elements are open circuited with $Z_S = 0$. In this case, all source voltage v_S is applied to the high-input resistance (r_π) of the BJT. Even though r_π is nonlinear, the voltage across it is constant. This constant voltage is multiplied by the nonlinear g_m. Therefore, g_m is the only nonlinear element, and the degeneration resistors linearize the g_m. The following equation describes the phenomenon:

$$i_O = -G_m v_S \tag{1a}$$

where

$$G_m = \frac{r_\pi g_m}{r_\pi + R_E g_m r_\pi + R_E + R_B} = \frac{\beta}{r_\pi + (1+\beta)R_E + R_B}. \tag{1b}$$

As shown in (1b), for a large R_E, G_m becomes α/R_E which has an α-dependent nonlinearity, and for a large R_B, G_m becomes

β/R_B which has a β nonlinearity. Since α is more linear than β, R_E is a more effective degeneration resistor than R_B. The linearization effects of R_E and R_B can be clearly visualized by using Voltera-series expansion of (1b)

$$\begin{aligned} G_m &= G_{mo} + \left.\frac{\partial G_m}{\partial r_\pi}\right|_{r_{\pi o}, g_{mo}} \Delta r_\pi + \left.\frac{\partial G_m}{\partial g_m}\right|_{r_{\pi o}, g_{mo}} \Delta g_m + \cdots \\ &= G_{mo} + \frac{\beta_o r_{\pi o} \frac{\Delta g_m}{g_{mo}} + (R_E + R_B)\beta_o \left(\frac{\Delta g_m}{g_m} + \frac{\Delta r_\pi}{r_{\pi o}}\right)}{(r_{\pi o} + (\beta_o + 1)R_E + R_B)^2} + \cdots. \end{aligned} \tag{2a}$$

Here, the subscript "o" refers to corresponding values at the bias point. Since g_m and $1/r_\pi$ are proportional to I_o, the variations are given by

$$\frac{\Delta g_m}{g_{mo}} = -\frac{\Delta r_\pi}{r_{\pi o}} = \frac{\Delta I_o}{I_o}. \tag{3}$$

Therefore, (2a) can be further simplified

$$G_m = G_{mo} + \frac{\beta_o r_{\pi o}\left(\frac{\Delta I_o}{I_o}\right)}{[r_{\pi o} + (\beta_o + 1)R_E + R_B]^2}. \tag{2b}$$

As can be seen from (2b), R_E is a more effective degeneration resistor than R_B, by a factor of $(\beta_o + 1)$.

This physical picture becomes complicated at a high frequency. The junction capacitances are not open circuited. The emitter–base junction impedance is not high, and the source impedance Z_S is usually conjugate matched to the input impedance of the device. Many studies at a high frequency indicate that C_{bc} is the major nonlinear element of the bipolar transistor [9]–[13] and should be linearized. This is accomplished by using a thin collector layer, which is fully depleted at a bias voltage, or by using a thick low-doped collector layer, which is depleted by the injected electron charges [13]. In those cases, C_{bc} becomes constant. When the C_{bc} nonlinearity is eliminated, the linearity of the bipolar transistor improves considerably, even though it has strong nonlinear elements.

We studied the linear characteristics of a bipolar transistor using a Volterra-series analysis. The results of our study for the circuit with linearized C_{bc} can be summarized as follows. For a constant input voltage v_S, the output current is given by

$$i_O = \frac{-Z_\pi g_m}{Z_{IN} + Z_S} v_S = \frac{-g_m}{g_\pi + j\omega C_{\text{diff}} + j\omega C_{\text{depl}}} \frac{v_S}{Z_{IN} + Z_S}. \tag{4}$$

Here, Z_π is the junction impedance of $(r_\pi || C_{\text{diff}} || C_{\text{depl}})$, and Z_{IN} is the input impedance given by $(R_B + Z_\pi + R_E(1 + Z_\pi g_m))$. Because $g_\pi (=1/r_\pi)$, C_{diff}, and g_m are linearly proportional to i_C, their nonlinear behaviors are identical. Therefore, (4) indicates that i_O is significantly linearized by the device internal characteristics, i.e., r_π and C_{diff} nonlinearities are canceled by g_m nonlinearity. Although the origin of C_{depl} nonlinearity is different, it can be partially canceled by g_m nonlinearity. Moreover, there are significant degeneration impedances, as shown in the denominator of (4). This is the reason for the high linearity of the bipolar transistor.

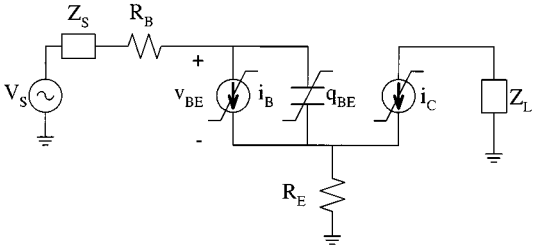

Fig. 2. HBT nonlinear equivalent circuit model.

Our calculation shows that if the base and collector ideality factors are identical, r_π and C_{diff} nonlinearities are completely canceled out by the g_m nonlinearity. The nonlinear current sources from r_π, C_{diff} and C_{depl} are connected to the parallel circuit of Z_π and the remaining part of the input circuit. Therefore, $Z_\pi/(Z_{IN} + Z_S)$ portions of the nonlinear currents generated by the nonlinearities are not delivered to the output, and the portion of g_m cannot be canceled out. The residual g_m nonlinearity is equivalent to the low frequency g_m nonlinearity, with high degeneration resistances given in (1b). In short, the major nonlinear source of HBT is C_{bc}. If C_{bc} is linearized, g_m with a large degeneration impedance is the major nonlinear source. C_{depl} nonlinearity cannot be completely canceled and becomes significant at a high frequency. The exponential nonlinear sources are internally canceled. In the following sections, we will give detailed analysis results.

III. Nonlinear Circuit Model of HBT

The simplified equivalent circuit of HBT used for our analysis is shown in Fig. 2. The base and collector nonlinear current sources are represented as i_B and i_C, respectively. Further, the base–emitter nonlinear capacitances appear as a charge q_{BE}. C_{bc} is assumed to be linearized for a constant capacitance and is omitted for nonlinear circuit analysis. This model includes all important nonlinearities and is sufficient to represent the essential nonlinear properties of HBT.

The nonlinear elements are represented by the third-order expansion of the Taylor series. Under a small-signal condition, the base nonlinear current source can be expanded in the vicinity of its bias point, yielding

$$i_B = I_{SB}\left[\exp\left(\frac{v_{BE}}{\eta_B V_T}\right) - 1\right] \tag{5}$$

$$i_b = \frac{I_B}{\eta_B V_T} v_{be} + \frac{I_B}{2\eta_B^2 V_T^2} v_{be}^2 + \frac{I_B}{6\eta_B^3 V_T^3} v_{be}^3 \tag{6}$$

$$\equiv g_1 v_{be} + g_2 v_{be}^2 + g_3 v_{be}^3 \tag{7}$$

where I_{SB} represents the saturation current, η_B is the ideality factor of the base current, I_B is dc base current, and V_T is thermal voltage, and i_b and v_{be} are the small-signal components of i_B and v_{BE}, respectively. Here, the coefficient g_1 $(=1/r_\pi)$ is linearized junction conductance.

The nonlinear current source at the base–collector junction i_C is given by

$$i_C = I_{SC}\left[\exp\left(\frac{v_{BE}}{\eta_C V_T}\right) - 1\right] \tag{8}$$

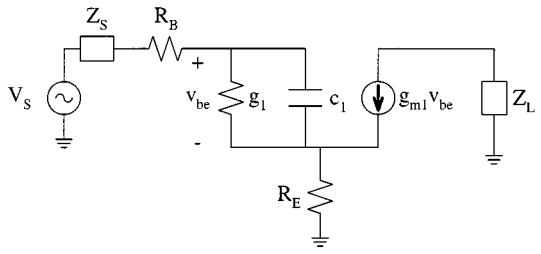

Fig. 3. HBT linear circuit for fundamental component analysis.

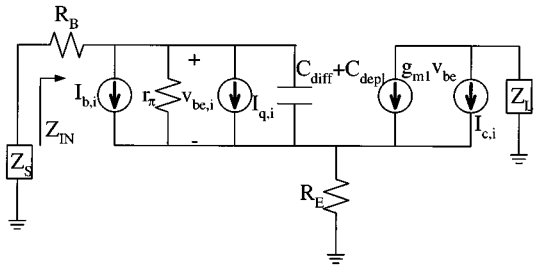

Fig. 4. HBT equivalent circuits for the second-order ($i = 2$) and third-order ($i = 3$) intermodulation analyses.

where I_{SC} and η_C represent the saturation current and ideality factor of the collector current, respectively. The collector nonlinear current source is also expanded as

$$i_c = \frac{I_C}{\eta_C V_T} v_{be} + \frac{I_C}{2\eta_C^2 V_T^2} v_{be}^2 + \frac{I_C}{6\eta_C^3 V_T^3} v_{be}^3 \tag{9}$$

$$\equiv g_{m1} v_{be} + g_{m2} v_{be}^2 + g_{m3} v_{be}^3 \tag{10}$$

where I_C is dc collector current, and i_c is the small-signal component of i_C. The coefficient, g_{m1} is equivalent to g_m.

The stored charge at the base–emitter junction, q_{BE}, is the sum of diffusion and depletion charges

$$q_{BE} = \tau_B i_C + \tau_E i_B + q A_E X_N N_E \tag{11}$$

where τ_B is the base transit time of the minority carrier, and τ_E is the emitter transit time, and is assumed to be comparable to τ_B. A_E is the emitter area, X_N is the depletion width of the emitter, and N_E is the doping concentration of the emitter. It can be also expanded as follows:

$$q_{be} = (C_{\text{diff}} + C_{\text{depl}}) v_{be} + \left(\frac{I_C}{2\eta_C^2 V_T^2} \tau_B + \frac{I_B}{2\eta_B^2 V_T^2} \tau_E + \frac{C_{\text{depl}}}{4(V_{bi} - V_{BE})} \right) v_{be}^2 + \left(\frac{I_C}{6\eta_C^3 V_T^3} \tau_B + \frac{I_B}{6\eta_B^3 V_T^3} \tau_E + \frac{C_{\text{depl}}}{8(V_{bi} - V_{BE})^2} \right) v_{be}^3 \tag{12}$$

$$\equiv c_1 v_{be} + c_2 v_{be}^2 + c_3 v_{be}^3 \tag{13}$$

where

$$C_{\text{depl}} = A_E \sqrt{\frac{q \epsilon_E \epsilon_B N_E P_B}{2(\epsilon_E N_E + \epsilon_B P_B)(V_{bi} - V_{BE})}}$$

and

$$C_{\text{diff}} = \frac{I_C}{\eta_C V_T} \tau_B + \frac{I_B}{\eta_B V_T} \tau_E.$$

For simplicity, depletion approximation is used. V_{bi} is built-in potential of base–emitter junction and V_{BE} is the base–emitter dc bias voltage. q_{be} is the small-signal component of q_{BE}. c_1 is the base–emitter junction capacitance $C_\pi (= C_{\text{depl}} + C_{\text{diff}})$.

IV. Second-Order Harmonic Analysis

The linear equivalent circuit of the HBT used for the first-order analysis is shown in Fig. 3. The first-order equation for the base-to-emitter voltage V_{be,ω_2} at the excitation frequency ω_2 can be expressed by

$$V_{be,\omega_2} = \frac{Z_\pi}{Z_{IN} + Z_S} V_{S,\omega_2}. \tag{14}$$

The second harmonic circuit used for our analysis is shown in Fig. 4. From the Volterra-series analysis given in Appendix I, the output current $I_{O,2\omega_2}$ at the second harmonic frequency is given by

$$\begin{aligned} I_{O,2\omega_2} &= A Z_{\pi,2\omega_2} \frac{g_m}{2r_\pi} \left(\frac{1}{2V_T \eta_C} - \frac{1}{2V_T \eta_B} \right) V_{be,\omega_2}^2 \\ &+ A Z_{\pi,2\omega_2} g_m \frac{j\omega_2 C_{\text{diff}}}{(\beta+1)} \left(\frac{1}{2\eta_C V_T} - \frac{1}{2\eta_B V_T} \right) V_{be,\omega_2}^2 \\ &+ A Z_{\pi,2\omega_2} g_m j\omega_2 C_{\text{depl}} \left(\frac{1}{2\eta_C V_T} - \frac{1}{4(V_{bi} - V_{BE})} \right) V_{be,\omega_2}^2 \\ &+ B \frac{g_m}{4\eta_C V_T} V_{be,\omega_2}^2 \end{aligned} \tag{A11}$$

where the coefficients A and B are given in (A12a) and (A12b) of Appendix I. Here, A is the portion of nonlinear currents from r_π, C_{diff}, and C_{depl} nonlinear sources flowing into Z_π and the portion is multiplied by g_m. Therefore, it cancels g_m nonlinearity. B is the portion of the nonlinear current, which flows into the source side and the portion of g_m nonlinearity cannot be canceled. In the input circuit, the feedback term $(R_E Z_\pi g_m)$ does not contribute to any harmonic generations.

The first term in (A11) originates from the cancellation of r_π and g_m nonlinearities. If the ideality factors of the current sources are identical, the second-order IM distortion currents are completely removed. The second term shows the cancellation between C_{diff} and g_m nonlinearities with the same behavior. The third term, generated from C_{depl} nonlinearity, can be canceled by g_m nonlinearity, but cannot be completely eliminated due to the different origin of sources. The last term is the residual g_m nonlinear portion. The coefficient Bg_m of the last term is identical to the highly degenerated g_m nonlinearity equation at the low frequency given in (1b). It can be expressed at a low frequency as

$$Bg_m = \frac{Z_{\pi,2\omega_2}}{Z_{IN,2\omega_2} + Z_{S,2\omega_2}} g_m \cong \frac{r_\pi g_m}{r_\pi + g_m r_\pi R_E + R_E + R_B}. \tag{15}$$

For the numerical calculation of the nonlinear components of HBT, we used the model parameters of the 3×20 μm^2

TABLE I
MODEL PARAMETERS OF HBT

Symbol	Value	Symbol	Value
I_E	16 mA	V_{BE}	1.60 V
I_B	0.39 mA	β	68
η_B	1.7	Z_L	150 Ω
η_C	1.0	Δf	1 MHz
g_1	0.0089	τ_B	8.72×10^{-13} s
g_2	0.1006	C_{depl}	4.3×10^{-13} F
g_3	0.7620	g_{m1}	0.6027
c_1	9.63×10^{-13}	g_{m2}	11.6350
c_2	1.42×10^{-11}	g_{m3}	149.7427
c_3	2.05×10^{-10}	R_B	8 Ω
V_{bi}	1.627 V	R_E	2 Ω

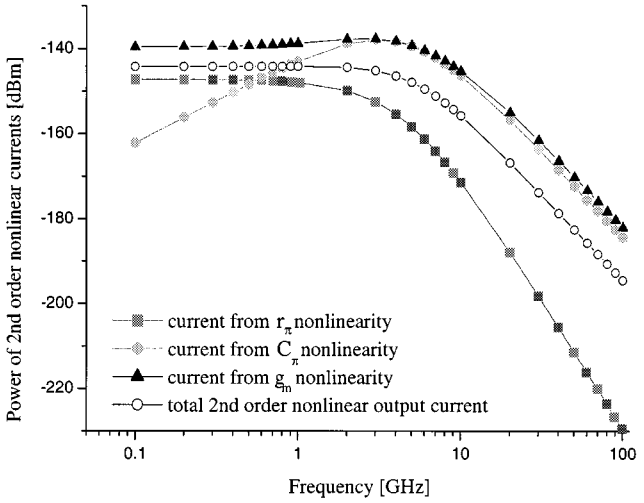

Fig. 5. Second harmonic currents at the output from each nonlinear source.

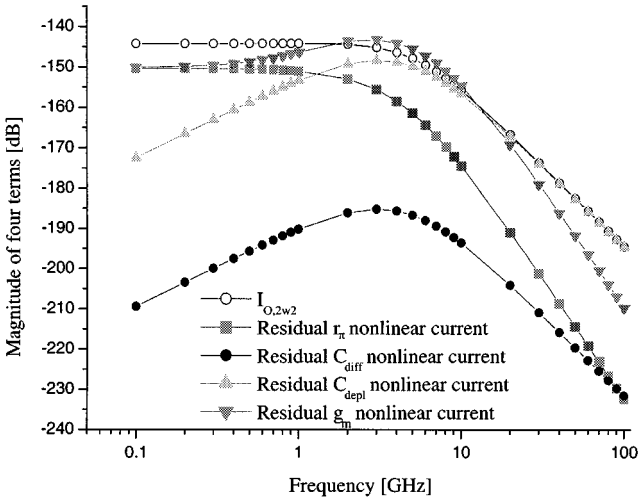

Fig. 6. Magnitude of four terms composing $I_{O,\,2\omega_2}$ in (A11).

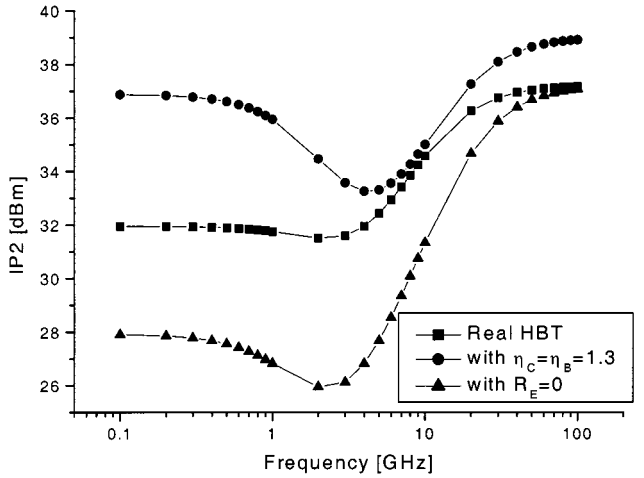

Fig. 7. IP2 levels of HBT calculated using the model parameters.

emitter HBT built at Pohang University of Science and Technology (POSTECH), Pohang, Korea. This device can deliver approximately 13 dBm of power. The parameters are summarized in Table I. For the calculation, Z_S and $Z_{S,\,2\omega_2}$ are adjusted to have impedance matching at the fundamental and harmonic frequencies and the input power is -60 dBm. Fig. 5 shows the second harmonic currents of the HBT at rf frequencies. As shown, $|I_{O,\,2\omega_2}|^2$, is much less than $|I_{c,\,2\omega_2}|^2$ (harmonics from g_m nonlinearity) for the overall frequency. $|I_{O,\,2\omega_2}|^2$ is about 5 dB less than $|I_{c,\,2\omega_2}|^2$ at a low frequency, and is about 12 dB lower at a high frequency. It is the result of a partial cancellation of $I_{c,\,2\omega_2}$ by $I_{b,\,2\omega_2}$ (harmonics from r_π nonlinearity) and $I_{q,\,2\omega_2}$ (harmonics from C_π). At a low frequency, $I_{b,\,2\omega_2}$ is larger than $I_{q,\,2\omega_2}$, but at a higher frequency, the situation is reversed. In addition, all currents start to decrease from about 3 GHz, because Z_π starts to decrease due to the capacitance effect. Fig. 6 shows the frequency-dependent values of the four terms of $I_{O,\,2\omega_2}$ in (A11). The cancellation between $C_{\rm diff}$ and g_m nonlinearities is significant for all frequencies, and the dominant nonlinear sources are r_π and g_m for a low frequency, and are $C_{\rm depl}$ and g_m for a high frequency. At a low frequency, the perfect cancellation of r_π nonlinearity by g_m nonlinearity using identical ideality factors can enhance the second-order intercept point (IP2) of the HBT.

We have calculated IP2 of our HBT and the same HBTs with some modifications. The results are shown in Fig. 7. The IP2 level of the HBT is flat below 1 GHz. Above 1 GHz, as $C_{\rm depl}$ nonlinearity becomes larger than r_π, and the IP2 level slightly decreases with frequency. However, as the portion B decreases with a frequency of about 4 GHz, the IP2 level rapidly increases and finally becomes constant. In the case of identical ideality factors of 1.3, the IP2 level is improved significantly at low frequencies, because r_π nonlinearity is perfectly canceled out by some portion of g_m nonlinearity. At higher frequencies, the depletion capacitance nonlinearity is dominant and the linearity improvement is minimal. For an AlGaAs/GaAs HBT, η_C of the graded E–B junction HBT is 1.0, while that of the abrupt junction HBT is from 1.1 to 1.3 [16]. Further, the η_B of an HBT with unpassivated extrinsic base region is around from 1.3 to 1.6, while that of a passivated HBT is near 2.0 [17]. Therefore, the unpassivated HBT with abrupt junction can have almost identical η_B and η_C, and can enhance IP2. However, the surface recombination is dispersive around the frequencies [18], and some care should be taken. The IP2 level for an HBT with $R_E = 0$ is also calculated. As expected, the IP2 level is reduced because the emitter degeneration has been removed.

V. Third-Order Harmonic Analysis

We performed a similar analysis for the third-order intermodulation (IM3). The detailed sequence of analysis for the circuit given in Fig. 4 is described in Appendix II. The third-order output current $I_{O,\,2\omega_2-\omega_1}$ is given by

$$
\begin{aligned}
&I_{O,\,2\omega_2-\omega_1}\\
&= D\frac{g_m}{r_\pi}\left[\left(\frac{1}{8\eta_C^2V_T^2}-\frac{1}{8\eta_B^2V_T^2}\right)+C\left(\frac{1}{2\eta_CV_T}-\frac{1}{2\eta_BV_T}\right)\right]\\
&\cdot V_{be,\,\omega_2}^2V_{be,\,\omega_1}^* + Dg_mj(2\omega_2-\omega_1)\frac{C_{\text{diff}}}{(1+\beta)}\\
&\cdot\left[\left(\frac{1}{8\eta_C^2V_T^2}-\frac{1}{8\eta_B^2V_T^2}\right)+C\left(\frac{1}{2\eta_CV_T}-\frac{1}{2\eta_BV_T}\right)\right]\\
&\cdot V_{be,\,\omega_2}^2V_{be,\,\omega_1}^* + Dg_mj(2\omega_2-\omega_1)C_{\text{depl}}\\
&\cdot\left[\left(\frac{1}{8\eta_C^2V_T^2}-\frac{3}{32(V_{bi}-V_{BE})^2}\right)\right.\\
&\quad\left.+C\left(\frac{1}{2\eta_CV_T}-\frac{1}{4(V_{bi}-V_{BE})}\right)\right]\\
&\cdot V_{be,\,\omega_2}^2V_{be,\,\omega_1}^* + Eg_m\left(\frac{1}{8\eta_C^2V_T^2}+C\,\frac{1}{2\eta_CV_T}\right)V_{be,\,\omega_2}^2V_{be,\,\omega_1}^*
\end{aligned}
\tag{A22}
$$

where the coefficients C, D and E are given in Appendix II. The D and E have the comparable meanings of A and B in the second-order analysis case.

The third-order output IM current in (A22) has a very similar form to the second-order one. The first term of the equation indicates that r_π nonlinearity is partially canceled by g_m nonlinearity, and it can be perfectly canceled for matched ideality factors. The second term of (A22) indicates that the diffusion charge part is also canceled by g_m nonlinearity. The third term shows that the distortion signal generated from the depletion capacitance is again incompletely canceled by some portion of that which is generated from the g_m nonlinearity. The last term is residual g_m nonlinearity and the degeneration resistances can effectively reduce it.

Fig. 8 shows the magnitude of the third order nonlinear currents of our HBT at RF frequencies. The basic behaviors are quite similar to that of the second-order case. At a low frequency, the nonlinear output current components from g_m and r_π nonlinearities are larger than $I_{O,\,2\omega_2-\omega_1}$. Because of the internal nonlinearity cancellation mechanism, $|I_{O,\,2\omega_2-\omega_1}|^2$ is approximately 10 dB less than the power of the nonlinear output current from g_m nonlinearity for the overall frequencies. Fig. 9 shows the frequency dependent values of the four terms of $I_{O,\,2\omega_2-\omega_1}$ in (A22). The cancellations between r_π and g_m, and C_{diff} and g_m nonlinearities are quite good for all frequencies. Therefore, the dominant nonlinear sources for all frequencies are C_{depl} and g_m. The nonlinear current from C_{depl} becomes comparable to g_m term at 2 GHz and above. At a low frequency (below 2 GHz), g_m nonlinearity with a large degeneration resistor creates IM3. Between 2∼20 GHz, IM3 are generated by C_{depl} and g_m nonlinearities. At higher frequencies, the dominant source is C_{depl}. Complete cancellation of C_{diff} and

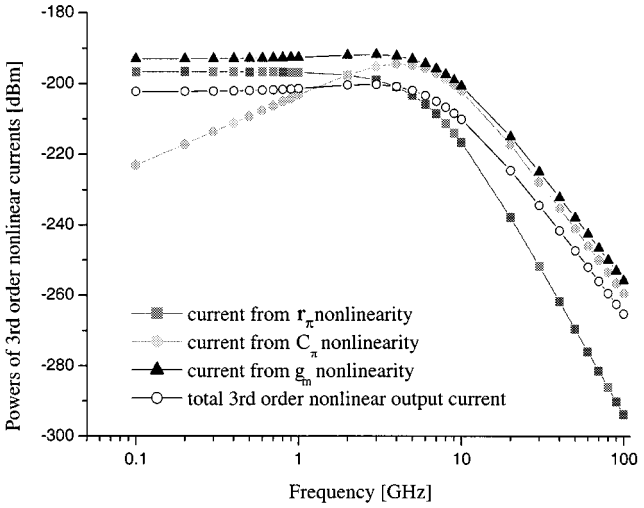

Fig. 8. Third-order nonlinear currents at the output from each nonlinear source.

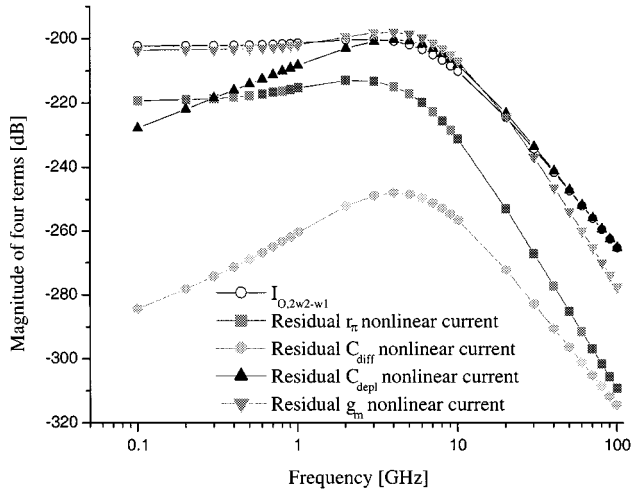

Fig. 9. Magnitude of four terms composing $I_{O,\,2\omega_2-\omega_1}$ in (A22).

r_π nonlinearities by g_m nonlinearity using identical ideality factors does not have any significant impact because they are rather small quantities.

We also examined the degeneration effects of the emitter and base resistances. Fig. 10 illustrates the surface of the IP3 level of HBT for various R_E and R_B at 2 GHz. For $R_E = 0\ \Omega$, as R_B increases, the IP3 level of HBT monotonously increases, following the degeneration of β nonlinearity. In the case of $R_E \neq 0$, the effect of R_B is negligible and R_E is the dominant factor, following the degeneration of α nonlinearity. The maximum IP3 of HBT is obtained at $R_E = 5\ \Omega$ and $R_B = 0\ \Omega$, which is 28.2 dBm. As R_E increases further, the IM3 signal decreases. However, the larger R_E reduces not only the IM3 signal but also the fundamental signal, and an optimum value of R_E is about 5 Ω in our case. These degeneration resistors should be designed to consider both the thermal ballast effect and linearization. A study for optimum R_B and R_E design is currently under investigation.

As can be seen from C of (A17) and (A22), the third-order IM currents are dependent on the second harmonic impedances of $Z_{S,\,2\omega_2}$ and $Z_{S,\,\omega_2-\omega_1}$. We have calculated the IP3 of HBT for

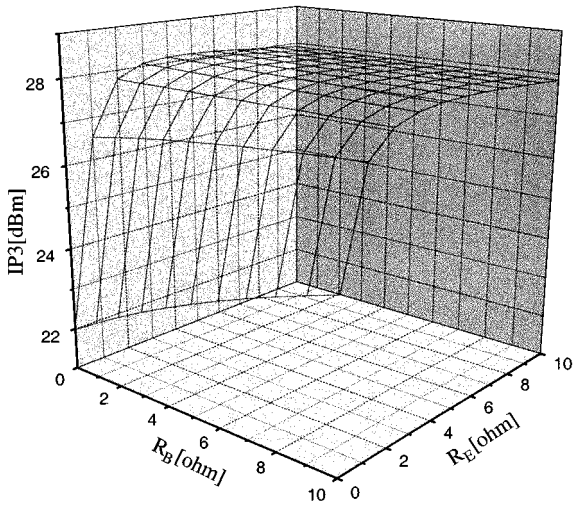

Fig. 10. Three-dimensional surface of IP3 level of our HBT as a function of R_E and R_B.

the various source terminations at the second harmonic frequencies. The IP3 can be enhanced by 3.5 dB by setting the second harmonic impedances of $Z_{S,\,2\omega_2} = 0$ and $Z_{S,\,\omega_2-\omega_1} = 0$, which are the optimum harmonic terminations.

VI. Conclusions

To clearly delineate the linear characteristics of an HBT, we developed an analytical nonlinear HBT model using Volterra-series analysis. Our model considers four nonlinearities: r_π, $C_{\rm diff}$, $C_{\rm depl}$, and g_m. The analysis reveals that there is an internal cancellation mechanism of nonlinearities in a BJT. The nonlinear currents from r_π and g_m, and $C_{\rm diff}$ and g_m nonlinearities are canceled quite well for all frequencies. Therefore, C_{bc} is the main nonlinear source. If C_{bc} is linearized, g_m is the main nonlinear sources of the HBT. g_m can be linearized using degeneration resistors. The degeneration resistor R_E is more effective than R_B for reducing g_m nonlinearity, since R_E linearizes the α-dependent nonlinearity while R_B the β dependent nonlinearity. The $C_{\rm depl}$ nonlinearity becomes important at a high frequency. This analysis also provides the dependency of the source second harmonic terminations on the linearity of HBT. The IP3 of the HBT improves considerably by setting the second harmonic impedances of $Z_{S,\,2\omega_2} = 0$ and $Z_{S,\,\omega_2-\omega_1} = 0$.

Appendix I
Volterra-Series Analysis of the Second-Order Components

The harmonics can be found by means of a Volterra-series analysis. Fig. 4 shows the equivalent circuit for the second-order nonlinear analysis. The second-order intermodulation currents generated by the nonlinear base-emitter junction capacitance $I_{q,\,2}$, and by the nonlinear base and collector current sources $I_{b,\,2}$ and $I_{c,\,2}$ are given by

$$I_{q,\,2} = \tfrac{1}{4}\, c_2 \sum_{i=-2}^{2} \sum_{k=-2}^{2} V_{be,\,\omega_i} V_{be,\,\omega_k} j(\omega_i + \omega_k) \cdot \exp(j(\omega_i + \omega_k)t), \tag{A1}$$

$$I_{b,\,2} = \tfrac{1}{4}\, g_2 \sum_{i=-2}^{2} \sum_{k=-2}^{2} V_{be,\,\omega_i} V_{be,\,\omega_k} \cdot \exp(j(\omega_i + \omega_k)t), \tag{A2}$$

$$I_{c,\,2} = \tfrac{1}{4}\, g_{m2} \sum_{i=-2}^{2} \sum_{k=-2}^{2} V_{be,\,\omega_i} V_{be,\,\omega_k} \cdot \exp(j(\omega_i + \omega_k)t) \tag{A3}$$

where $V_{be,\,\omega_i}$ is the first-order voltage phasor of V_{be} at the excitation frequency ω_i. Thus, the second-order IM current source for the frequency of $2\omega_2$ is given by

$$I_{q,\,2\omega_2} = \tfrac{1}{2}\, j(2\omega_2) c_2 V_{be,\,\omega_2}^2 = j\omega_2 c_2 V_{be,\,\omega_2}^2 \tag{A4}$$

$$I_{b,\,2\omega_2} = \tfrac{1}{2}\, g_2 V_{be,\,\omega_2}^2 \tag{A5}$$

$$I_{c,\,2\omega_2} = \tfrac{1}{2}\, g_{m2} V_{be,\,\omega_2}^2. \tag{A6}$$

Performing a linear analysis of this circuit, we find the base-to-emitter junction voltage at the second harmonic as shown in (A7) at the bottom of this page.

The output current $I_{O,\,2\omega_2}$ at this second harmonic frequency is

$$I_{O,\,2\omega_2} = g_{m1} V_{be,\,2\omega_2} + I_{c,\,2\omega_2}. \tag{A8}$$

Substituting (A7) into (A8) gives

$$\begin{aligned} I_{O,\,2\omega_2} = {} & \frac{-g_{m1}(Z_{S,2\omega_2} + R_B + R_E) Z_{\pi,2\omega_2}}{Z_{IN,2\omega_2} + Z_{S,2\omega_2}}\, I_{b,\,2\omega_2} \\ & + \frac{-g_{m1}(Z_{S,2\omega_2} + R_B + R_E) Z_{\pi,2\omega_2}}{Z_{IN,2\omega_2} + Z_{S,2\omega_2}}\, I_{q,\,2\omega_2} \\ & + \frac{(Z_{\pi,2\omega_2} + Z_{S,2\omega_2} + R_B + R_E)}{Z_{IN,2\omega_2} + Z_{S,2\omega_2}}\, I_{c,\,2\omega_2}. \end{aligned} \tag{A9}$$

Equation (A9) is further simplified to

$$\begin{aligned} & I_{O,\,2\omega_2} \\ & = \frac{(Z_{S,2\omega_2} + R_B + R_E) Z_{\pi,2\omega_2}}{Z_{IN,2\omega_2} + Z_{S,2\omega_2}} \{-g_{m1} I_{b,\,2\omega_2} + g_1 I_{c,\,2\omega_2}\} \\ & \quad + \frac{(Z_{S,2\omega_2} + R_B + R_E) Z_{\pi,2\omega_2}}{Z_{IN,2\omega_2} + Z_{S,2\omega_2}} \\ & \quad \cdot \{-g_{m1} I_{q,\,2\omega_2} + j2\omega_2 c_1 I_{c,\,2\omega_2}\} \\ & \quad + \frac{Z_{\pi,2\omega_2}}{Z_{IN,2\omega_2} + Z_{S,2\omega_2}}\, I_{c,\,2\omega_2} \end{aligned} \tag{A10}$$

$$V_{be,\,2\omega_2} = \frac{-(Z_{S,2\omega_2} + R_B + R_E) Z_{\pi,2\omega_2} (I_{b,2\omega_2} + I_{q,2\omega_2}) - R_E Z_{\pi,2\omega_2} I_{c,2\omega_2}}{Z_{IN,2\omega_2} + Z_{S,2\omega_2}} \tag{A7}$$

$$= AZ_{\pi,2\omega_2}\frac{g_{m1}}{2r_\pi}\left(\frac{1}{2\eta_C V_T}-\frac{1}{2\eta_B V_T}\right)V_{be,\omega_2}^2 + AZ_{\pi,2\omega_2}g_{m1}\frac{j\omega_2 C_{\text{diff}}}{(\beta+1)}\left(\frac{1}{2\eta_C V_T}-\frac{1}{2\eta_B V_T}\right)V_{be,\omega_2}^2 + AZ_{\pi,2\omega_2}g_{m1}j\omega_2 C_{\text{depl}} \cdot\left(\frac{1}{2\eta_C V_T}-\frac{1}{4(V_{bi}-V_{BE})}\right)V_{be,\omega_2}^2 + B\frac{g_{m1}}{4\eta_C V_T}V_{be,\omega_2}^2 \quad \text{(A11)}$$

with

$$A=\frac{(Z_{S,2\omega_2}+R_B+R_E)}{Z_{IN,2\omega_2}+Z_{S,2\omega_2}} \quad \text{(A12a)}$$

$$B=\frac{Z_{\pi,2\omega_2}}{Z_{IN,2\omega_2}+Z_{S,2\omega_2}}. \quad \text{(A12b)}$$

APPENDIX II
VOLTERRA-SERIES ANALYSIS OF THE THIRD-ORDER COMPONENTS

Fig. 4 is applied to the calculation of the third-order IM components. Since this circuit is identical to the second order circuit, it can be analyzed in a similar manner. The third-order IM current sources at the interesting frequency of $2\omega_2-\omega_1$ are given by

$$I_{q,2\omega_2-\omega_1} = j(2\omega_2-\omega_1)\tfrac{3}{4}c_3 V_{be,\omega_2}^2 V_{be,\omega_1}^* + j(2\omega_2-\omega_1)c_2 \cdot[V_{be,2\omega_2}V_{be,\omega_1}^* + V_{be,\omega_2}V_{be,\omega_2-\omega_1}] \quad \text{(A13)}$$

$$= j(2\omega_2-\omega_1)\left[\tfrac{3}{4}c_3+c_2C\right]V_{be,\omega_2}^2 V_{be,\omega_1}^* \quad \text{(A14)}$$

$$I_{b,2\omega_2-\omega_1} = \left[\tfrac{3}{4}g_3+Cg_2\right]V_{be,\omega_2}^2 V_{be,\omega_1}^* \quad \text{(A15)}$$

$$I_{c,2\omega_2-\omega_1} = \left[\tfrac{3}{4}g_{m3}+g_{m2}C\right]V_{be,\omega_2}^2 V_{be,\omega_1}^* \quad \text{(A16)}$$

where C is shown in (A17) at the bottom of this page.

The third-order base–emitter voltage is calculated using the equation which is similar to the second-order voltage, as shown in (A18) at the bottom of this page.

$$C=-\left[\frac{(Z_{S,2\omega_2}+R_B+R_E)(g_2+j2\omega_2c_2)+R_Eg_{m2}}{2[1+(Z_{S,2\omega_2}+R_B+R_E)(g_1+j2\omega_2c_1)+R_Eg_{m1}]} + \frac{(Z_{S,\omega_2-\omega_1}+R_B+R_E)(g_2+j(\omega_2-\omega_1)c_2)+R_Eg_{m2}}{1+(Z_{S,\omega_2-\omega_1}+R_B+R_E)(g_1+j(\omega_2-\omega_1)c_1)+R_Eg_{m1}}\right] \quad \text{(A17)}$$

$$V_{be,2\omega_2-\omega_1} = \frac{-(Z_{S,2\omega_2-\omega_1}+R_B+R_E)Z_{\pi,2\omega_2-\omega_1}(I_{b,2\omega_2-\omega_1}+I_{q,2\omega_2-\omega_1})-R_EZ_{\pi,2\omega_2-\omega_1}I_{c,2\omega_2-\omega_1}}{Z_{IN,2\omega_2-\omega_1}+Z_{S,2\omega_2-\omega_1}} \quad \text{(A18)}$$

$$I_{O,2\omega_2-\omega_1} = g_{m1}V_{be,2\omega_2-\omega_1}+I_{c,2\omega_2-\omega_1} \quad \text{(A19)}$$

$$= \frac{-g_{m1}(Z_{S,2\omega_2-\omega_1}+R_B+R_E)Z_{\pi,2\omega_2-\omega_1}(I_{b,2\omega_2-\omega_1}+I_{q,2\omega_2-\omega_1})-g_{m1}R_EZ_{\pi,2\omega_2-\omega_1}I_{c,2\omega_2-\omega_1}}{Z_{IN,2\omega_2-\omega_1}+Z_{S,2\omega_2-\omega_1}} + \frac{[Z_{\pi,2\omega_2-\omega_1}+(Z_{S,2\omega_2-\omega_1}+R_B+R_E)+R_Eg_{m1}Z_{\pi,2\omega_2-\omega_1}]I_{c,2\omega_2-\omega_1}}{Z_{IN,2\omega_2-\omega_1}+Z_{S,2\omega_2-\omega_1}} \quad \text{(A20)}$$

$$= \frac{(Z_{S,2\omega_2-\omega_1}+R_B+R_E)Z_{\pi,2\omega_2-\omega_1}}{Z_{IN,2\omega_2-\omega_1}+Z_{S,2\omega_2-\omega_1}}\left[\frac{3}{4}(g_1g_{m3}-g_3g_{m1})+C(g_1g_{m2}-g_2g_{m1})\right]V_{be,\omega_2}^2V_{be,\omega_1}^* + \frac{(Z_{S,2\omega_2-\omega_1}+R_B+R_E)Z_{\pi,2\omega_2-\omega_1}}{Z_{IN,2\omega_2-\omega_1}+Z_{S,2\omega_2-\omega_1}} \cdot\left[\tfrac{3}{4}j(2\omega_2-\omega_1)(c_1g_{m3}-c_3g_{m1})+j(2\omega_2-\omega_1)C(c_1g_{m2}-g_{m1}c_2)\right]V_{be,\omega_2}^2V_{be,\omega_1}^* + \frac{Z_{\pi,2\omega_2-\omega_1}}{Z_{IN,2\omega_2-\omega_1}+Z_{S,2\omega_2-\omega_1}}\left(\frac{3}{4}g_{m3}+Cg_{m2}\right)V_{be,\omega_2}^2V_{be,\omega_1}^* \quad \text{(A21)}$$

$$= D\frac{g_{m1}}{r_\pi}\left[\left(\frac{1}{8\eta_C^2V_T^2}-\frac{1}{8\eta_B^2V_T^2}\right)+C\left(\frac{1}{2\eta_CV_T}-\frac{1}{2\eta_BV_T}\right)\right]V_{be,\omega_2}^2V_{be,\omega_1}^* + Dg_{m1}j(2\omega_2-\omega_1)\frac{C_{\text{diff}}}{(1+\beta)}\left[\left(\frac{1}{8\eta_C^2V_T^2}-\frac{1}{8\eta_B^2V_T^2}\right)+C\left(\frac{1}{2\eta_CV_T}-\frac{1}{2\eta_BV_T}\right)\right]V_{be,\omega_2}^2V_{be,\omega_1}^* + Dg_{m1}j(2\omega_2-\omega_1)C_{\text{depl}} \cdot\left[\left(\frac{1}{8\eta_C^2V_T^2}-\frac{3}{32(V_{bi}-V_{BE})^2}\right)+C\left(\frac{1}{2\eta_CV_T}-\frac{1}{4(V_{bi}-V_{BE})}\right)\right]V_{be,\omega_2}^2V_{be,\omega_1}^* + Eg_{m1}\left(\frac{1}{8\eta_C^2V_T^2}+C\frac{1}{2\eta_CV_T}\right)V_{be,\omega_2}^2V_{be,\omega_1}^* \quad \text{(A22)}$$

Further, the third-order IM output current at this frequency is given by (A19)–(A22), shown at the bottom of the previous page, where

$$D = \frac{(Z_{S,2\omega_2-\omega_1} + R_B + R_E)Z_{\pi,2\omega_2-\omega_1}}{Z_{IN,2\omega_2-\omega_1} + Z_{S,2\omega_2-\omega_1}} \tag{A23a}$$

$$E = \frac{Z_{\pi,2\omega_2-\omega_1}}{Z_{IN,2\omega_2-\omega_1} + Z_{S,2\omega_2-\omega_1}}. \tag{A23b}$$

REFERENCES

[1] C. T. M. Chang and H.-T. Yuan, "GaAs HBT's for high-speed digital integrated circuit applications," *Proc. IEEE*, vol. 81, pp. 1727–1743, Dec. 1993.

[2] P. M. Asbeck, M. F. Chang, J. J. Corcoran, J. F. Jensen, R. N. Nottenburg, A. Oki, and H. T. Yuan, "HBT application prospects in the US: Where and when?," in *IEEE GaAs IC Symp. Tech. Dig.*, Monterey, CA, Oct. 1991, pp. 7–10.

[3] G.-B. Gao, D. J. Roulston, and H. Morkoc, "Design study of AlGaAs/GaAs HBTs," *IEEE Trans. Electron Devices*, vol. 37, pp. 1199–1208, May 1990.

[4] M. E. Kim, A. K. Oki, J. B. Camou, P. D. Chow, B. L. Nelson, D. M. Smith, J. C. Canyon, C. C. Yang, R. Dixit, and B. R. Allen, "12–40 GHz low harmonic distortion and phase noise performance of GaAs HBTs," in *IEEE GaAs IC Symp. Tech. Dig.*, Nov. 1988, pp. 117–120.

[5] S. A. Maas, B. L. Nelson, and D. L. Tait, "Intermodulations in HBTs," *IEEE Trans. Microwave Theory Tech.*, vol. 40, no. 3, pp. 442–448, Mar. 1992.

[6] T. Iwai, S. Ohara, H. Yamada, Y. Yamaguchi, K. Imanishi, and K. Joshin, "High efficiency and high linearity InGaP/GaAs HBT power amplifiers: Matching techniques of source and load impedance to improve phase distortion and linearity," *IEEE Trans. Electron Devices*, vol. 45, pp. 1196–1200, June 1998.

[7] K. W. Kobayashi, J. C. Cowles, L. T. Tran, A. Gutierrez-Aitken, M. Nishimoto, J. H. Elliott, T. R. Block, A. K. Oki, and D. C. Streit, "A 44-GHz-high IP3 InP HBT MMIC amplifier for low DC power millimeter-wave receiver applications," *IEEE J. Solid-State Circuits*, vol. 34, pp. 1188–1194, Sept. 1999.

[8] A. Samelis and D. Pavlidis, "Mechanisms determining third order intermodulation distortion in AlGaAs/GaAs HBTs," *IEEE Trans. Microwave Theory Tech.*, vol. 40, pp. 2374–2380, Dec. 1992.

[9] N. L. Wang, W. J. Ho, and J. A. Higgins, "AlGaAs/GaAs HBT linearity characteristics," *IEEE Trans. Microwave Theory Tech.*, vol. 42, pp. 1845–1850, Oct. 1994.

[10] J. Lee, W. Kim, T. Rho, and B. Kim, "Intermodulation mechanism and linearization of AlGaAs/GaAs HBTs," *IEEE Trans. Microwave Theory Tech.*, vol. 45, pp. 2065–2072, Dec. 1997.

[11] P. Asbeck, "HBT linearity and basic linearization approaches," presented at the IEEE MTT-S Int. Microwave Symp. Workshop, Baltimore, MD, June 1998.

[12] M. Iwamoto, T. S. Low, C. P. Hutchinson, J. B. Scott, A. Cognata, X. Qin, L. H. Camnitz, P. M. Asbeck, and D. C. D'Avanzo, "Influence of collector design on InGaP/GaAs HBT linearity," in *IEEE MTT-S Int. Microwave Symp. Dig.*, Boston, MA, June 2000, pp. 757–760.

[13] W. Kim, S. Kang, K. Lee, M. Chung, Y. Yang, and B. Kim, "The effects of Cbc on the linearity of AlGaAs/GaAs power HBT," *IEEE Trans. Microwave Theory Tech.*, vol. 49, pp. 1270–1276, July 2001.

[14] N. Wiener, *Nonlinear Problems in Random Theory*. New York: Technol. Press, 1958.

[15] S. A. Maas, *Nonlinear Microwave Circuits*. Norwood, MA: Artech House, 1988.

[16] W. Liu, *Handbook of III–V Heterojunction Bipolar Transistor*. New York: Wiley, 1998.

[17] W. Liu and J. Harris, "Diode ideality factor for surface recombination current in AlGaAs/GaAs heterojunction bipolar transistors," *IEEE Trans. Electron Devices*, vol. 39, pp. 2726–2732, Dec. 1992.

[18] B. Ihn, J. Lee, T. M. Roh, Y. S. Kim, and B. Kim, "Surface recombination related frequency dispersion of current gain in AlGaAs/GaAs HBTs," *Electron. Lett.*, vol. 34, no. 10, pp. 1031–1033, 1998.

Woonyun Kim (S'95–M'01) was born in Seoul, Korea, in 1970. He received the B.S., M.S., and Ph.D. degrees in electronic and electrical engineering from Pohang University of Science and Technology, Pohang, Korea, in 1994, 1996, and 2001, respectively.

In 2001, he joined the RFIC Design Group, System LSI Business, Samsung Electronics Company Ltd., Kiheung, Korea, where he is involved in research and development of RFIC designs for wireless communications.

Sanghoon Kang was born in Pusan, Korea, in 1972. He received the B.S. and M.S. degrees in electrical engineering in 1996 and 1998, respectively, from Pohang University of Science and Technology, Pohang, Korea, where he is currently working toward the Ph.D. degree.

His research interests include CMOS RFIC design, in particular, mixer linearity and noise.

Kyungho Lee was born in Miryang, Korea, in 1975. He received the B.S. degree in electronics and electrical engineering in 1999 from Kyungpook National University, Taegu, Korea, and the M.S. degree in electronics and electrical engineering in 2001 from Pohang University of Science and Technology, Pohang, Korea, where he is currently working toward the Ph.D. degree.

His research interests include the development of high-speed devices, including GaAs-based and InP-based HBTs, and their applications.

Minchul Chung received the B.S. and M.S. degrees in electronic and electrical engineering in 1997 and 1999, respectively, from Pohang University of Science and Technology, Pohang, Korea, where he is currently working toward the Ph.D. degree.

His research interests are the design and fabrication of GaAs-based low-noise HBTs and MMICs, including low-phase-noise HBT oscillators.

Jongchan Kang was born in Cheonan, Korea, in 1973. He received the B.S. degree in electronic engineering from Han-Yang University, Ansan, Korea, in 2000. He is currently working toward the Ph.D. degree at Pohang University of Science and Technology, Pohang, Korea.

His research interests are linearization of power HBTs and design of power amplifiers for handsets.

Bumman Kim (S'77–M'78–SM'97) received the Ph.D. degree in electrical engineering from Carnegie-Mellon University, Pittsburgh, PA, in 1979.

From 1978 to 1981, he was engaged in fiber-optic network component research at GTE Laboratories Inc. In 1981, he joined the Central Research Laboratories, Texas Instruments Incorporated, where he was involved in development of GaAs power FETs and MMICs. He has developed a large-signal model of a power FET, dual-gate FETs for gain control, high-power distributed amplifiers, and various millimeter-wave MMICs. In 1989, he joined Pohang University of Science and Technology, Pohang, Korea, where he is a Professor in the Electronic and Electrical Engineering Department, and Director of the Microwave Application Research Center, where he works on device and circuit technology for MMICs. Currently, he is a Visiting Professor of Electrical Engineering at California Institute of Technology, Pasadena. He has authored more than 100 published technical papers.

Dr. Kim is a member of the Korean Academy of Science and Technology and Academy of Engineering of Korea.